A Numerical Study of the Rock Pillar Failure Mechanisms

Ali Mortazavi[i]

ABSTRACT

Pillar design and stability analysis is an issue that is faced routinely in mining and civil industries. In mining operations, while the establishment of several mining levels is often necessary to ensure adequate production, it does result in formation of pillars that must be recovered under high stress conditions at later stages of excavation. Moreover, in civil infrastructures, such as underground power stations, waste repositories, warehouses, etc., design of remnant rock pillars is necessary and very common. Therefore, it is beneficial to develop guidelines that help in the design of rock pillars as well as to maintain their long-term stability. The aim of this paper was to delve into the mechanism involved in rock pillar loading process and failure mechanisms. The effects of pillar geometry, pillar and surrounding ground stiffness were investigated on pillar failure mechanism. A thorough numerical analysis was carried out to investigate the pillar deformation and failure process under natural loading conditions. Accordingly, the obtained results were compared against field data, from Canadian mining operations, published by various researchers. A fairly good match was obtained between the numerical findings and published field data.

KEYWORDS

Numerical modelling, failure analysis, pillar failure, rock mechanics, mining.

1. INTRODUCTION

Since the early days of opening underground excavations, pillars have been employed as an important support system in mining and civil infrastructures. Without pillars it is impossible to support the great weight of overburden material or withstand lateral pressures in deep underground openings. Pillars are used in a variety of underground operations such as mining operations and the construction of underground repositories and warehouses. In spite of a significant amount of research conducted, pillar failure still poses significant safety issues and occasionally places lives at risk. The intension of this paper is to carry out a detailed investigation of pillar failure mechanisms in hard rock situations and to help reduce the safety and economic hazards of pillar failures in underground infrastructures. A combination of numerical modelling and field data is used to develop an understanding of the important factors that control pillar failure, and to suggest guidelines for pillar design.

2. BACKGROUND

Knowledge of pillar strength is a requirement in determining the required safety factor for a given loading condition. The pillar load can be evaluated using either empirical or numerical techniques, but the in-situ pillar strength is generally unknown and much more difficult to determine. The pillar strength determined in the laboratory is not applicable to real field conditions. Laboratory-scale samples are much stronger than in-situ rock, and the laboratory test is an oversimplification of the real situation in terms of sample shape, size, loading condition, confinement, friction and other in-situ effects. This makes it difficult to make a realistic prediction of in-situ pillar strength based on laboratory results. Salamon [1] was the first author who proposed an empirical and semi-statistical approach for pillar strength calculation in South African coal mines. The data was gathered on all known cases of failed pillars in South Africa and a comparison was made between the depth and dimension of the failed and unfailed pillars. Accordingly, based on his analysis and fundamental principles indicated by the laboratory work, he derived an empirical formula for the strength of coal pillars as below:

$$\sigma = 7.2\frac{w^{0.46}}{h^{0.66}} \qquad (1)$$

i A. Mortazavi is with the Department of Mining and Metallurgical Engineering, Amirkabir University of Technology, Tehran, Iran (e-mail: mortazav@aut.ac.ir).

where σ is the pillar strength in *MPa* and w and h are pillar width and height (*m*), respectively.

Salmon's formula is given only for coal pillars of square shape. If the pillar is not square (i.e., rectangular or a parallelogram), the above formula should be modified and an equivalent pillar width should be determined. Alternative formulas are given by van der Merwe [5]. The pillar strength is strongly related to intact material strength and pillar *W/H* ratio as it can be seen from Salamon's formula. Geological parameters can also have major impacts on the strength achieved under various loading conditions. Rock mass classification techniques are useful tools in incorporating the effects of discontinuities in any geomechanical analysis. For example, the Hoek-Brown criterion may be used to estimate the rock mass uniaxial compressive strength from the uniaxial compressive strength of intact rock samples tested under laboratory conditions.

According to Esterhuizen [2], the effect of jointing on pillar strength can be accounted for by simply reducing the calculated strength of a pillar by an amount equal to the reduction in the seam strength predicted by classification methods. This would, however, reduce the strength of all pillars by an equal amount regardless of the width-to-height ratio. It seems inappropriate to apply a constant reduction in strength to pillars of different width-to-height ratios. For example, jointing is not likely to affect a pillar with a width-to-height ratio of 4:1 as severely as it would affect a pillar with a width-to-height ratio of 1:1. An alternative approach is to use numerical modelling to investigate the effects of jointing on the strength of pillars with varying width-to-height ratio. Esterhuizen [2] conducted an interesting numerical study of the effects of joint orientation on pillar strength. The modelling results were compared to Salamon's empirical formula results and a very good agreement was obtained between these two approaches. Furthermore, the effect of discontinuity dip was evaluated on the pillar strength. The results imply that pillars with large width-to-height ratios are less sensitive to the presence of joints. The results also showed that shear occurs along joints only in the outer portion of a pillar, up to a depth approximately equal to the height of the pillar.

A. Pillar loading mechanism

Assuming that each pillar carries its full share of the overburden load, the load being exerted on a pillar can be calculated as the weight of overburden material. This approach is valid when the excavation layout and the distribution of pillars within the excavated area are regular. From a theoretical point of view, as these pillars are loaded, they will undergo a transition through the following phases:

a) Virgin conditions
b) Stresses rising at the sides with core relatively unchanged
c) Sides fractured and failed and core stresses rising
d) Side fracture zones grow larger while core approaching yield conditions
e) Convergence of fractured zones
f) Gradual destressing of failed pillar

The above process has been demonstrated conceptually, numerically, and experimentally by many authors [3, 5, etc.]. As an example, experimental finding of Winton et al. [7] on pillar behaviour is presented in Figure 1. Looking at this figure initially the stresses are concentrated at pillar sides. With increase in loading, pillar sides fail leading to stress drop in failed regions. This process continues leading to the growth of fracture zone toward pillar core. Eventually if the loading process continues pillar core approaches yield condition and will result in failure and destressing of pillar.

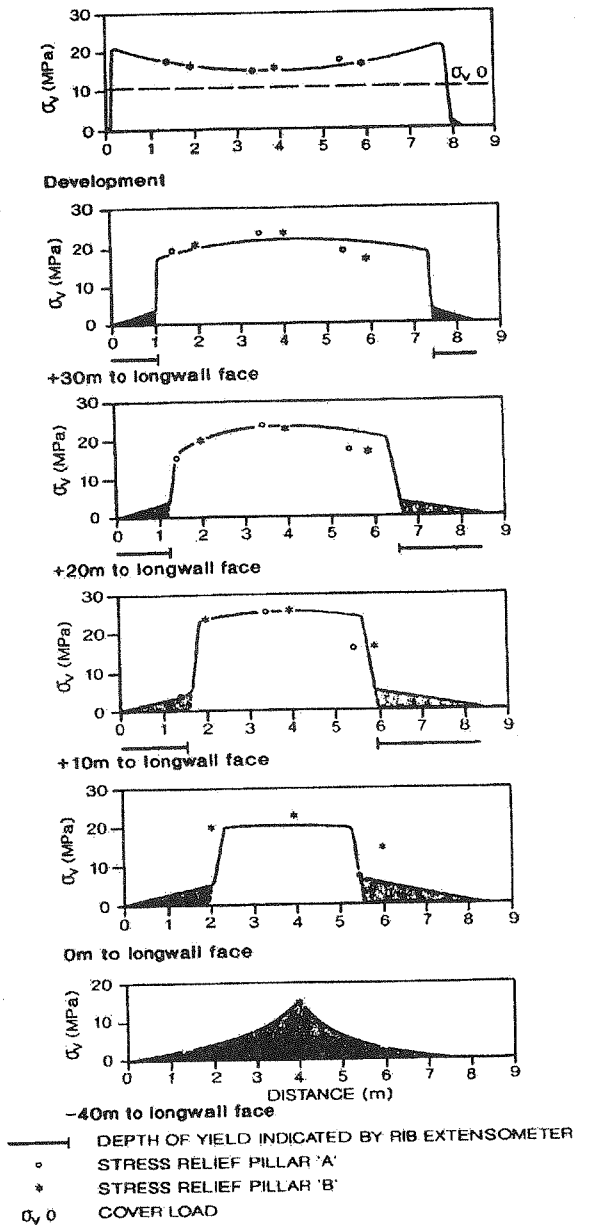

Figure 1: Example of small pillar monitoring studies indicating pillar stress history [7].

With regard to extreme difficulties associated with pillar strength and load evaluations, numerical modelling is then the only alternative to assess the pillar behaviour. One of the main objectives of this paper is to assess the load-displacement behaviour of the host rock-pillar system numerically.

B. The concept of pillar-host rock stiffness interaction and its role in pillar failure

The interaction between a pillar and its surrounding rock can be explained by considering the uniaxial testing of a specimen in the laboratory. Considering the actual pillar in-situ, the deformation of the pillar depends on the forces exerted upon it by the floor and roof. Figure 2-a shows a typical load-displacement curve for a pillar. As the pillar is loaded, it is compressed elastically along the line *OA* until its peak load-bearing capacity P_{max} is reached. At this point, the pillar may be internally fractured and if loading continues in a controlled manner along post peak deformation path *AB*, the pillar has the capacity to support loads less than P_{max}. The post-peak deformation of the pillar is affected by the stiffness of the surrounding area and that determines whether pillar will go through a stable or unstable failure. Figure 2-b demonstrates a situation where the local ground stiffness (indicated by thick line) is less than the pillar stiffness. As the pillar deforms further, a force P_H is exerted on the pillar by the roof and floor whereas at this point pillar is capable of carrying load P_J. This extra loading of the pillar leads to its catastrophic failure. The energy stored in roof and floor (area *AHDC* that is the available energy to be transferred to the pillar) is larger than the energy required to deform the pillar (area *AJDC*). The excess energy (shaded area) causes the unstable failure of the pillar.

Figure 2-c illustrates a situation in which local ground stiffness is higher than the pillar stiffness. Curve *OAB* shows the deformation path of the pillar and line AG demonstrates the stiffness of the roof and floor. In this case, a given increase in the pillar deformation in its post-elastic range results in application of a P¬L load from roof and floor to the pillar. The energy associated with this loading (area *ALDC*) is less than the energy that pillar can take (work being done on the pillar) i.e., area *AKDC*. Hence, the pillar will follow its natural load-deformation path and will fail in a controlled manner. The local ground stiffness depends on fixed parameters such as the overburden characteristics and geology and rock properties. The greater the proportion of stiffer rock types such as massive sandstone and dolerite in the overburden layers, the stiffer the system will be. However, the presence of discontinuities such as faults can affect the stiffness of even the stiffest rock types [5].

In spite of the fact that the stiffness concept is very important in describing the failure process, experimental determination of ground or pillar in-situ stiffness is very difficult and not feasible practically. Therefore, the use of numerical methods is the only viable alternative to study the pillar failure process.

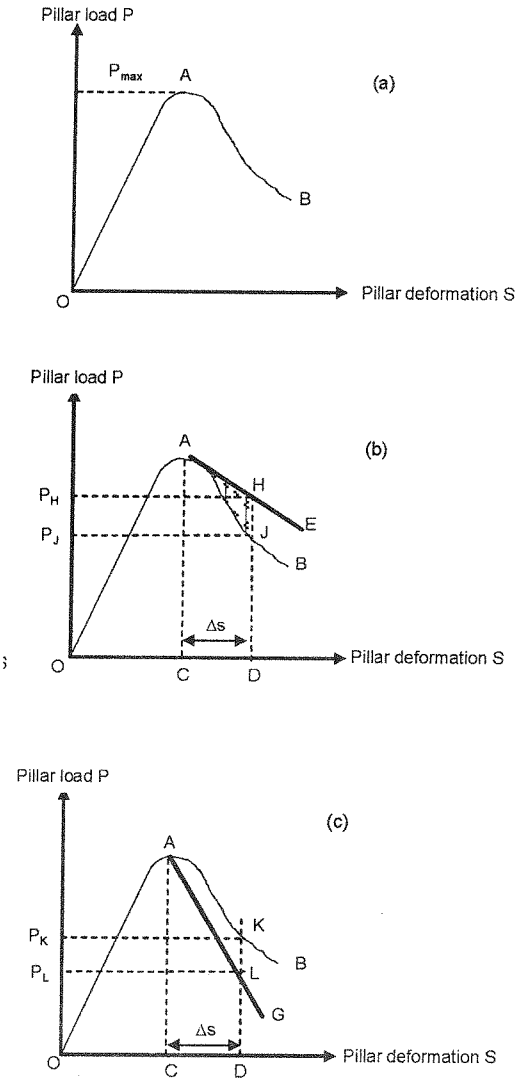

Figure 2: a) Typical load-deformation curve for a pillar, b) Interaction of pillar and rock with low stiffness, c) Interaction of pillar and rock mass with high stiffness.

3. Numerical Modelling

A. Modelling strategy and Input data

A 2-D Distinct Element Code was used for the numerical analysis. The code allows for complete non-linear modelling in the post-elastic failure range of rock material. The dimensions used in the model were selected based on typical dimensions of rock pillars used in Canadian underground mining operations. This enabled the comparison of numerical results with actual field data which is published in literature. A narrow steeply dipping orebody was simulated under cut & fill excavation conditions. The orebody thickness (the pillar "height" for a near-vertical orebody) was varied from 5 to 30 m and numerical results were determined for each case. Excavation was started at the mid-height as well as the

lowest portion of the orebody in the up-dip direction. At the end of the excavation sequence, a pillar was left at the middle part of the orebody. The concern was to study the behaviour of this pillar as large-scale rock convergence and sudden release of strain energy occur as the final dimensions of the pillar and excavated area are approached. Figure 3 demonstrates the complete geometry of the model used in the numerical analysis. Figure 4 illustrates the geometry of a pillar (*W/H* ratio of 1:1) during the excavation process. A single set of input data was used during the numerical analysis. Table 1 presents the input data used in the analysis. The same input data were used for all runs to enable the comparisons of the results. These input parameters were selected with regards to the existing data on rock properties collected from various Canadian mining operations. The strain-softening/hardening model employed within the program allowed capturing the non-linear behaviour of the pillar in the post elastic range. Using this model, the cohesion, friction angle, dilation angle, and tensile strength can change as a function of plastic strain experienced within the material. In the presented numerical analysis, it is assumed that the cohesion value of the material is changing as a function of plastic strain.

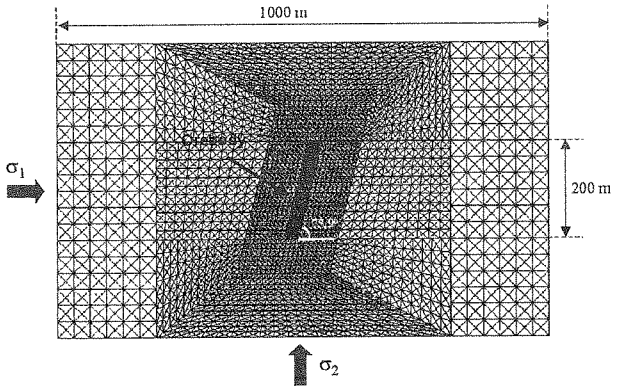

Figure 3: Geometry of model used in the numerical simulations.

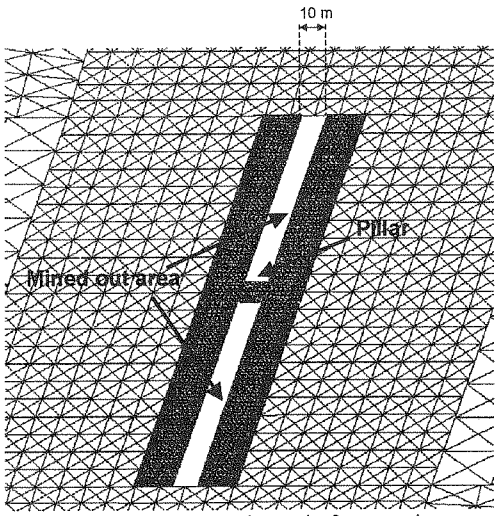

Figure 4: Pillar geometry at the end of excavation process.

TABLE 1

ROCK PROPERTY DATA USED IN THE NUMERICAL ANALYSIS.

Bulk modulus (Pa)	Shear modulus (Pa)	Density (kg/m^3)	Cohesion (Pa)	Tensile strength (Pa)	Friction angle (°)	Dilation angle (°)
2.33e10	1.40e1	2700	25e6	12.5e6	30	10

B. Numerical modelling results

With regard to the discussion given in Section 4, first it was decided to numerically evaluate the effects of local ground stiffness. As mentioned earlier, experimental evaluation of ground stiffness effects is very difficult and expensive. Hence, numerical techniques are currently the best tools to evaluate this issue and to shed some light on it. Accordingly, a series of simulations was carried out, to determine the local ground stiffness. During all runs, a set of monitoring points was placed at various locations within the pillar as well as the host rock. Then, stress and deformation values were monitored during various stages of excavation. Figure 5 illustrates the approximate location of monitoring points. The calculated local ground stiffness for various pillar geometries is illustrated in Figure 6. This figure shows that the local ground stiffness, which is reflected by the slope of the line, is essentially independent of the pillar height, and by extension, is independent of the pillar width/height ratio.

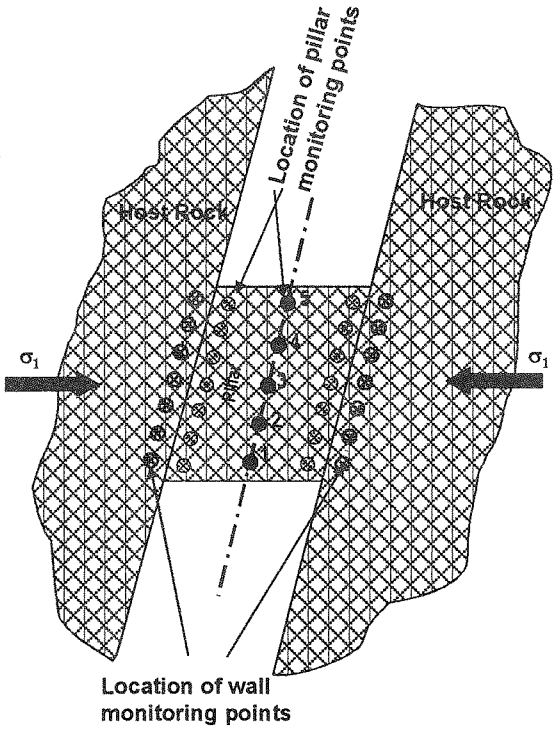

Figure 5: Location of stress and deformation monitoring points.

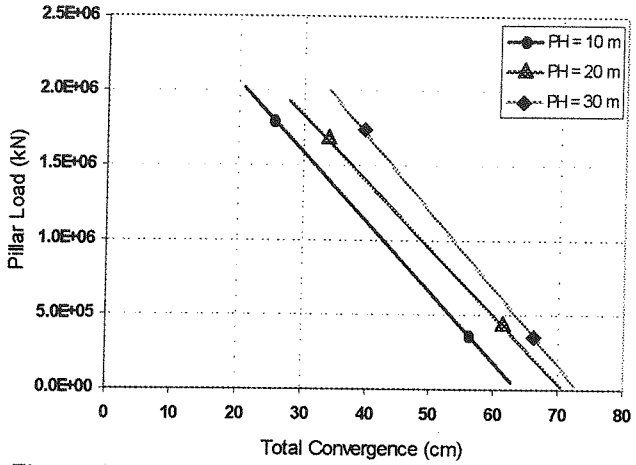

Figure 6: Local ground stiffness curve (pillar width – 10 m).

The objective of the analysis presented in this section is to determine the complete pillar load-displacement curve, at a given pillar geometry, as excavation proceeds (i.e., pillar is gradually loaded). In this set of analyses, all parameters were kept unchanged except for the pillar geometry. For a given pillar height, excavation was conducted in the orebody dip direction, thus loading the pillar in a gradual manner as the various cuts were excavated. Since the objective was to have a detailed study of the load distribution and change within the pillar during the excavation process, and to quantify the results, excavation was conducted in a somewhat artificial manner, i.e., up-dip and down-dip away from the pillar. This allowed for a gradual and more symmetric loading of the pillar due to excavation. The reason for the approach taken here in the modelling analyses is to allow for a gradual loading of a given pillar geometry, from both sides simultaneously, and evaluate the loading behaviour of the pillar as a function of its geometry (*W/H* ratio). Additionally, it is conceptually easier to evaluate the post failure behaviour of the pillar and interpret the variation of stress within the pillar. During the excavation process the maximum principal stress, (assumed to be in the *x* direction) was monitored continuously. The location of monitoring points was selected such that the influence of pillar end effect (e.g., confinement offered by frictional effects of pillar-host rock contact and as a result increase in pillar strength) was minimal. Figure 5 shows a schematic geometry of the pillar along with the locations of the points at which stress was monitored. Accordingly, numerical results were obtained for various pillar dimensions. It should be borne in mind that for all considered pillar heights, a pillar width of 10 m was considered. To be concise, the obtained results for one pillar geometry (*W/H* Ratio = 1:1) is presented in this section and the summary results for all conducted analyses are presented at the end of the paper. Figure 7 illustrates the load and deformation history during the excavation process. Here it can be seen that there is a significant drop in load as the pillar suddenly fails during excavation step 5 (after 3000 time steps). Figure 8 demonstrates the pillar load-displacement curve during the excavation process.

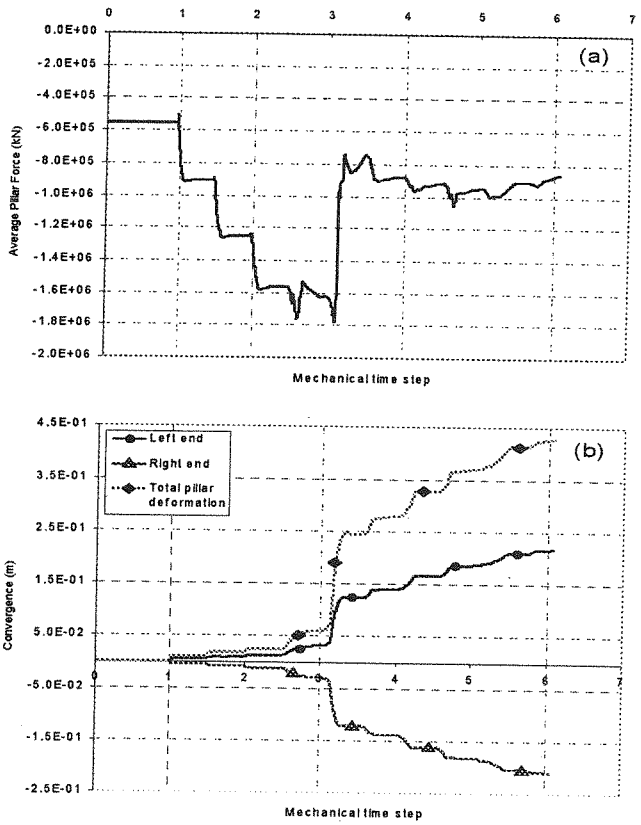

Figure 7: Pillar load (a), and deformation (b) history as excavation proceeds.

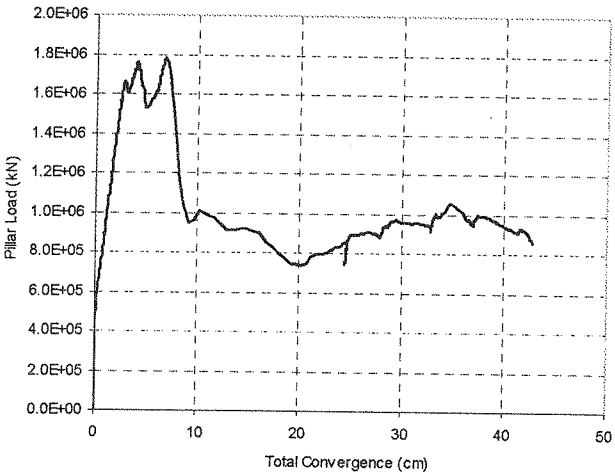

Figure 8: Pillar load-displacement curve (*W:H* – 1:1).

The pattern of stress change within the pillar, as the excavation process advances, is also plotted in Figure 9. This figure shows the magnitude of maximum principal stress in the pillar during various excavation steps. Once again, as excavation starts on both sides of the pillar, elastic stresses start to build up at the pillar edges and stress concentrations rise at these points. However, in this case, in comparison to smaller pillar heights, there is not significant stress concentration at the pillar edge. This

shows that as the pillar height increases (smaller *W/H* ratio), the pillar starts the yielding process right from the beginning rather than storing stress in an elastic manner and then failing. Towards the end of the excavation, the high stresses shift to the pillar centre. Figure 9 also shows that at the last stage of excavation, the pillar started to fail in the centre as well. This can be understood from a drop in stress magnitude at this stage.

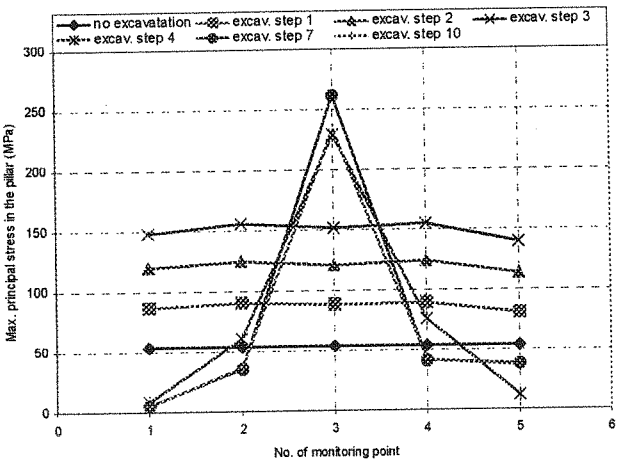

Figure 9: Pattern of stress change within the pillar during the excavation process.

C. Summary and discussion

Pillar *W/H* ratio is an important aspect of pillar design. The behaviour of a pillar is generally governed by its stiffness and strength properties. The stiffness and uniaxial strength of the pillar controls the initial behaviour of the body against applied loading and basically defines the onset of failure in the material. Once the failure has commenced, it is the geometrical component of the stiffness that plays a role in the deformational behaviour and basically controls the rest of the failure process. Hence, from a safe pillar design point of view, *W/H* ratio is probably the most important parameter to be considered. This section is devoted to summarizing the analyses conducted on pillar behaviour as function of geometry (i.e., *W/H* ratio). Figure 10 illustrates the load-displacement curve obtained for various pillar geometries. For the sake of argument, the ground stiffness curve determined for the base case pillar geometry (1:1 *W/H* ratio) is also plotted on the same figure. With regard to Figure 10, at larger *W/H* ratios pillar load-bearing capacity will significantly increase. This is a universally agreed concept in the literature. With increases in *W/H* ratio more confinement will be offered to the pillar core, due to increase in width (more mass of material surrounding the pillar), leading to an increase in its strength.

Additionally, with an increase in width, the pillar-host rock contact area will increase and, hence, further frictional resisting forces will be mobilized at the contact area. These frictional forces introduce a restraining and confining effect to the pillar in particular at the top and bottom portions. As pillar width increases, this confinement will propagate and penetrate into the pillar centre from both top and bottom portions of the pillar. Accordingly, the full pillar height will be affected by this confinement, leading to an increase in its strength. As can be seen from the plots, as *W/H* ratio reduces, the pillar load bearing capacity drops. It is interesting to note that once the *W/H* ratio is reduced to a certain value (in this study less than 0.5 *W/H* ratio), the maximum load-bearing capacity of the pillar remains almost the same. This shows that at lower *W/H* ratios, it is the inherent material strength that governs the failure and since strength properties are the same for all cases, a similar peak load is achieved for all cases. In other words, at low *W/H* ratios the geometry has no strengthening effect and confinement offered by frictional forces will vanish. Comparing the slopes of the pillar behaviour curves (in the elastic region) also shows the role of geometry in defining the pillar stiffness.

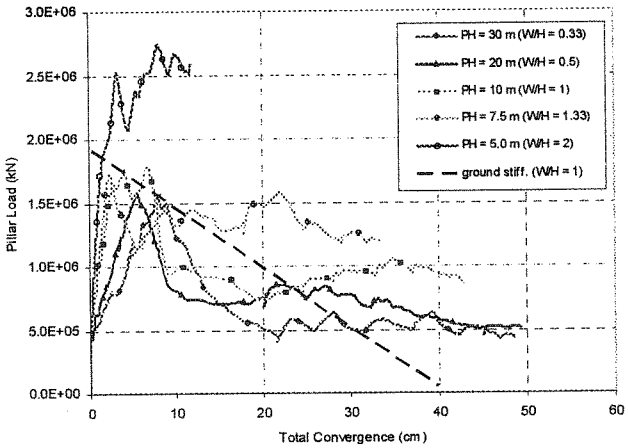

Figure 20: Load-displacement curve for various pillar geometries.

4. Comparison of Numerical Results and Field Data

A. Red Lake Mine data

This data is a summary of back analyses of pillars in seven "high burst prone" and five "low burst prone" regions which were in production at Goldcorp Inc.'s Campbell Red Lake (CRL) Mine, Canada between 1991 and 1994. The back analyses involved the comparison of four Canadian empirical failure criteria [4, 8, 9, 10]. The Red Lake data was included in a CANMET publication [6].

B. Elliot Lake (Nordic Mine) data

The uranium mines in the Elliot Lake mining district were mined using a room and pillar method. Pillars were generally long enough to be considered as two-dimensional. At times, these pillars became burst-prone, and many were mined in such a configuration that they were relatively highly stressed. The orebody was a relatively brittle conglomerate, hosted between layers of

quartzite. In this set of data, for a given pillar height and width, pillar strength is calculated from Hedley's strength formula. Based on underground observations, pillar condition was defined as: Rock splitting, fractured, taking weight (e.g., still carrying load), or failed and a safety factor was determined for each case. Accordingly, field data from Red Lake and Elliot Lake mining districts were normalized and plotted against obtained numerical results. The summary of all data is illustrated in Figure 11. From Figure 11 it can be seen that the peak and residual strength envelopes obtained from numerical analysis fit the data reasonably well, in that they seem to place bounds on the very scattered field data. This makes sense if one accepts that in the field, one is likely to encounter a number of pillars whose condition is not known. Some of these may be failed completely, and some may still have intact cores. From a visual assessment it is not always possible to tell the condition of the pillar, and it is often difficult to differentiate between a "failed" and an "unstable" pillar, both of which are obviously showing signs of taking load.

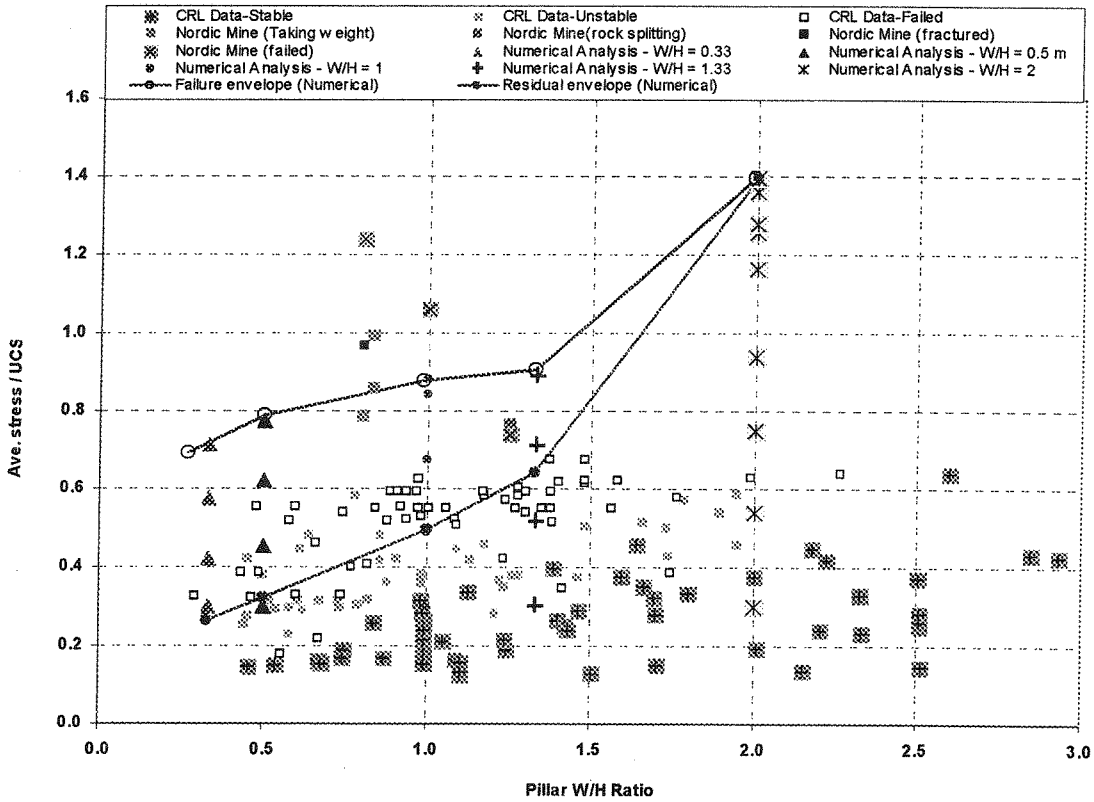

Figure 31: Load-displacement curve for various pillars.

5. Conclusions

The local ground stiffness concept is an important factor, since it explains the dynamic failure behaviour of a pillar. If the local ground stiffness is less than the slope of the pillar post-peak strain softening curve, then the potential for a violent failure exists. If the loading system is stiffer than the pillar material, there is no excess energy to give up during pillar failure. It is fairly easy to determine the local ground stiffness numerically, as has been done in this research. The span of opening was originally thought to be an important factor affecting the local ground stiffness. According to conducted numerical analysis, the local ground stiffness is relatively independent of the span of the opening. However, the elastic properties of the host rock strongly influence the local ground stiffness, with softer (lower modulus) host rock being more prone to violent failure.

Pillar *W/H* ratio is an important factor influencing pillar behaviour, since this shape factor governs the pillar stiffness and strength properties. The stiffness and uniaxial strength of the pillar controls the initial behaviour against applied loading and defines the onset of failure in the pillar material. Once failure has commenced, the geometry of the pillar plays a role in the deformational behaviour and controls the rest of the failure process. Hence, from a safe pillar design viewpoint, the *W/H* ratio is probably the most important parameter to be considered.

The conducted analyses show that as *W/H* ratio reduces, the pillar load bearing capacity drops. Once the *W/H* ratio is reduced below 0.5 (*W/H* ratio), the maximum load-bearing capacity of the pillar remains almost the same. Thus, at lower *W/H* ratios, it is the inherent material strength that governs the failure. In other words, at low *W/H* ratios the geometry has no strengthening effect and confinement offered by frictional forces vanishes. Comparing the slopes of the pillar behaviour curves, in the elastic region, (Figure 10) also shows the role of geometry in defining the pillar stiffness. The results shown in Figure

10 indicate that at high W/H ratios, pillar behaviour was:

a) very stiff in the elastic range and demonstrating a high load-bearing capacity,
b) maintaining the load bearing capacity and storing energy in post elastic range ($W/H = 2$) or sudden failure ($W/H = 1.33$ and 1), and
c) softening behaviour along with eventual hardening of material in the final stages of post-elastic behaviour.

The peak and residual strength envelopes obtained from numerical analysis fitted the available field data reasonably well, in that they seem to place bounds on the very scattered field data. This is promising since in the field, one is likely to encounter a number of pillars whose condition is not known. Some pillars may be failed completely, and some may still have intact cores. In brief, the conducted analysis provides a qualitative design chart which can be used in the design of rock pillars in underground infrastructures.

6. References

[1] M.D.G Salamon, A.H. Munro, "A study of the strength of coal pillars," *The Journal of South African Institute of Mining and Metallurgy*, Sep.1967.

[2] G.S. Esterhuizen, "Investigations into the effect of discontinuities on the strength of coal pillars," *The Journal of South African Institute of Mining and Metallurgy*, pp. 57-61, March/April 1997.

[3] G. York, "Numerical modelling of the yielding of a stabilizing pillar/foundation system and a new design consideration for stabilizing pillar foundations," *The Journal of South African Institute of Mining and Metallurgy*, pp. 281-297, Oct. 1998.

[4] D.G.F. Hedley, F. Grant, "Stope and pillar design for the Elliot Lake uranium mines," *CIM Bull.*, vol. 65, pp. 37-44, 1972.

[5] J.N. Van der Merwe, "Practical coal mining strata control: A guide for managers and supervisors at all levels," *Published by Itasca Africa Ltd.*, 1998.

[6] CANMET Report, "Development of empirical design techniques in burst prone ground at A.W. White Mine," CANMET project No. 1-9180, Vol. I, 1995.

[7] J.G. Winton, "Experience of field measurements and computer simulation methods for pillar design," in *Proc. of the 2nd Int. Workshop on Coal Pillar Mechanics and Design, US Department of Health and Human Services, Vail, Colorado*, pp 49-61, 1999.

[8] E. Hoek, E.T. Brown, "The Hoek-Brown failure criterion- a 1988 update," in *Rock Engineering for Underground Excavations, Proc. 15th Can. Rock Mech. Symp., University of Toronto*, pp. 31-38, 1988.

[9] Lunder, "Development of pillar design guidelines for hard rock mining operations," in *16th CIM District 6 Meeting, Vancouver, B.C.*, 1994.

[10] M.R. Hudyma, "Rib pillar design in open stope mining," M.Sc. Thesis, University of British Columbia, 1988.